Journal of ELECTRONIC MATERIALS, Vol. 49, No. 7, 2020
https://doi.org/10.1007/s11664-020-08127-5

Performance of a Thermoelectric Module Based on *n*-Type $(La_{0.12}Sr_{0.88})_{0.95}TiO_{3-\delta}$ and *p*-Type $Ca_3Co_{4-x}O_{9+\delta}$

NIKOLA KANAS,[1,5] GUNSTEIN SKOMEDAL,[2] TEMESGEN DEBELO DESISSA,[3] ARMIN FELDHOFF,[4] TOR GRANDE,[1] KJELL WIIK,[1] and MARI-ANN EINARSRUD[1]

1.—Department of Materials Science and Engineering, NTNU Norwegian University of Science and Technology, Trondheim, Norway. 2.—Department of Engineering Sciences, University of Agder, Grimstad, Norway. 3.—Department of Materials Science and Engineering, Adama Science and Technology University, Adama, Ethiopia. 4.—Institute of Physical Chemistry and Electrochemistry, Leibniz University Hannover, Hannover, Germany. 5.—e-mail: nikola.kanas@ntnu.no

Here, we present the performance of a thermoelectric (TE) module consisting of *n*-type $(La_{0.12}Sr_{0.88})_{0.95}TiO_3$ and *p*-type $Ca_3Co_{4-x}O_{9+\delta}$ materials. The main challenge in this investigation was operating the TE module in different atmospheric conditions, since *n*-type has optimum TE performance at reducing conditions, while *p*-type has optimum at oxidizing conditions. The TE module was exposed to two different atmospheres and demonstrated higher stability in N_2 atmosphere than in air. The maximum electrical power output decreased after 40 h when the hot side was exposed to N_2 at 600°C, while only 1 h at 400°C in ambient air was enough to oxidize $(La_{0.12}Sr_{0.88})_{0.95}TiO_3$ followed by a reduced electrical power output. The module generated maximum electrical power of 0.9 mW ($\sim$ 4.7 mW/cm^2) at 600°C hot side and $\Delta T \sim 570$ K in N_2, and 0.15 mW ($\sim$ 0.8 mW/cm^2) at 400°C hot side and $\Delta T \sim 370$ K in air. A stability limit of $Ca_3Co_{3.93}O_{9+\delta}$ at $\sim$ 700°C in N_2 was determined by in situ high-temperature x-ray diffraction.

Key words: Oxide thermoelectric module, $(La_{0.12}Sr_{0.88})_{0.95}TiO_{3-\delta}$, $Ca_3Co_{4-x}O_{9+\delta}$, thermal stability, oxidation, electrical power output

INTRODUCTION

Thermoelectric (TE) materials based on oxides are promising alternatives to the state-of-the-art non-oxide thermoelectric materials due to stability at high temperatures. In spite of moderate performance, oxide TE modules have the potential to replace batteries as a power source for sensors operating at high temperatures in oxidizing and mild reducing atmospheres, and as such also enable wireless transfer of data from the sensors.[1–4] Oxide TE modules may also be used at high temperatures as heat flux monitors, which is highly relevant in the process industry.[5] Several oxide materials with *p*-type electrical conductivity have been reported, including $Ca_3Co_{4-x}O_{9+\delta}$ (CCO), which shows the highest performance. So far, the most promising oxide materials with *n*-type electrical conductivity are $Zn_{0.96}Al_{0.02}Ga_{0.02}O$, $CaMn_{0.98}Nb_{0.02}O_3$ and $La_{0.15}Sr_{0.775}TiO_{3-\delta}$ with figures of merit (zT) of 0.65 at 970°C (ambient air),[6] 0.32 at 790°C (ambient air)[7] and 0.41 at 700°C (5% H_2/N_2),[8] respectively. A high power factor of above 7 μW/cm K^2 is reported at 900°C for $In_{1.9}Sn_{0.05}Al_{0.05}O_3$ (air), also representing a promising *n*-type TE material.[9]

Pure $SrTiO_3$ is a dielectric material due to a large band gap (3.2 eV),[10] but the material demonstrates high *n*-type electrical conductivity at reducing conditions due to the introduction of oxygen vacancies and delocalized electrons caused by Ti^{3+} formation.

(Received December 18, 2019; accepted March 26, 2020; published online April 10, 2020)

In addition, donor doping with La on the A-site increases the electrical conductivity corresponding to a significant enhancement of zT.[8,11] $SrTiO_3$-based materials have rarely been used for fabrication of TE modules; however, 50 pairs of n-type $La_{0.035}Sr_{0.965}TiO_3$ and a non-oxide p-type $Ni_{0.9}Mo_{0.1}$ yielded 450 mW/cm^2 at thermal gradient (ΔT) 360 K under 5% H_2/Ar.[12]

$Ca_3Co_{4-x}O_{9+\delta}$ (p-type electrical conductivity) is stable up to 926°C in air,[13] and since the valence state of Co is strongly dependent on the partial pressure of oxygen, the stability is dependent on working conditions such as atmosphere and temperature. Due to the presence of two sub-lattices in $Ca_3Co_{4-x}O_{9+\delta}$, the Co ions in CoO_2 edge-sharing octahedra possess oxidation state +4, while those in the rock-salt Ca_2CoO_3 vary in oxidation state and induce variations in δ.[14] Enhanced stability of $Ca_3Co_{3.93}O_{9+\delta}$ in pure O_2 (up to $\sim$ 1070°C) has been reported,[15] while the stability in atmospheres with reduced pO_2 has not yet been reported. Notable improvement in electrical conductivity of $Ca_3Co_4O_{9+\delta}$ compared to $Ca_3Co_{3.98}O_{9+\delta}$ and $Ca_3Co_{4.02}O_{9+\delta}$ was reported for the single-phase materials, where the boundary for obtaining pure phase is between $Ca_3Co_{3.95}O_{9+\delta}$ (Ca:Co = 0.76) and $Ca_3Co_{4.05}O_{9+\delta}$ (Ca:Co = 0.74).[16] Accordingly, Ca:Co ratios below 0.74 will result in composite CCO with the presence of Co_3O_4, and reduced electrical conductivity[17] due to the poor conductivity of Co_3O_4.[18]

$SrTiO_3$-based TE materials require reducing atmosphere to maintain stable TE performance at elevated temperature. On the other hand, $Ca_3Co_{4-x}O_{9+\delta}$ demands oxidizing conditions to maintain the structure and an acceptable electrical conductivity.

These contradicting working conditions for the TE couple are challenging, and here we present an analysis of the stability and TE performance of a module consisting of p-type $Ca_3Co_{4-x}O_{9+\delta}$ and n-type $(La_{0.12}Sr_{0.88})_{0.95}TiO_{3-\delta}$ in N_2 and air, respectively. A discussion of the stability of the two materials in the two atmospheres is included. As a result of this investigation, essential insight with respect to the performance of the system is provided, as well as possible solutions to improve the performance of the module.

EXPERIMENTAL

Processing

$(La_{0.12}Sr_{0.88})_{0.95}TiO_{3-\delta}$ (LSTO) powder was synthesized by a solid-state reaction (SSR), where a precursor mixture of $SrCO_3$, TiO_2 and La_2O_3 (Inframat Advanced Materials, Manchester, CT, USA) was heat-treated at 1090°C for 7 h in air (Super Kanthal, chamber furnace). $Ca_3Co_{3.93}O_{9+\delta}$ powder was prepared by SSR (CCO-SSR) where a precursor mixture of $CaCO_3$ and Co_3O_4 (Inframat Advanced Materials, Manchester, CT, USA) was heat-treated at 880°C for 14 h in air (for more details see Ref. 15), and $Ca_3Co_{4-x}O_{9+\delta}$ by spray pyrolysis (CCO-SP) from aqueous nitrate solutions (CerPoTech AS, Norway). Different stoichiometries with different Ca:Co ratios were obtained. LSTO ceramics were prepared by cold isostatic pressing (200 MPa) followed by sintering in a tube furnace (Nabertherm) at 1300°C for 4 h under 5% H_2/Ar, while CCO-SP ceramics were prepared by spark plasma sintering (SPS) at 870°C and 50 MPa for 2 min. We recently showed that the SSR route, which usually gives microstructures with larger grains, results in better TE performance of LSTO ceramics,[19] while the opposite trend was observed for CCO,[15] hence different sintering techniques were used.

One leg each of CCO-SP and LSTO ceramics were ground to $\sim$ 3.4 mm in height and cut into a rectangular shape prior to assembling the TE modules. The surfaces of the legs facing the hot and cold sides were ground by 1200 SiC paper and coated with a $\sim$ 50 nm film of gold. The legs were then placed between silver foils, and silver paint was used on both the hot and the cold sides to ensure good bonding between the legs and the silver electrodes. The paint was cured in air at room temperature for 3 h before the module was tested.

Characterization

Thermal stability of CCO-SSR powder in N_2 was analyzed by high-temperature XRD (HT-XRD) (θ-2θ Bruker D8 Advance diffractometer) from ambient temperature to 800°C, with steps of 100°C followed by 30 min hold at each temperature. Thermogravimetric analysis (Netzsch STA 449 F3 Jupiter) of finely ground bulk CCO-SP, CCO-SSR powder and LSTO ceramics was carried out in a temperature range of 25–1100°C in N_2 (pre-vacuum) and air using a heating rate of 10 K/min. Bulk densities were determined by Archimedes measurement in isopropanol.

Characterization of the TE modules consisting of spark plasma as-sintered CCO-SP and as-sintered in 5% H_2/Ar LSTO ceramic legs was carried out in both N_2 (chamber flushed with N_2) and air for 120 h at maximum temperatures of 600 ($\Delta T \approx$ 570 K) and 450°C ($\Delta T \approx$ 420 K), respectively. The TE modules were rapidly heated (100 K/min), and measurements performed in air were recorded at several temperatures below 600°C (hot side) during short dwellings at each step. Measurements in air were performed at 130°C, 400°C and 450°C hot-side temperature. More details on the characterization of the thermoelectric modules is provided elsewhere.[20]

RESULTS AND DISCUSSION

Characterization of TE Modules

Characterization of the TE modules in the two different atmospheres is presented in Fig. 1, where the maximum electrical power output (P_{max}), open

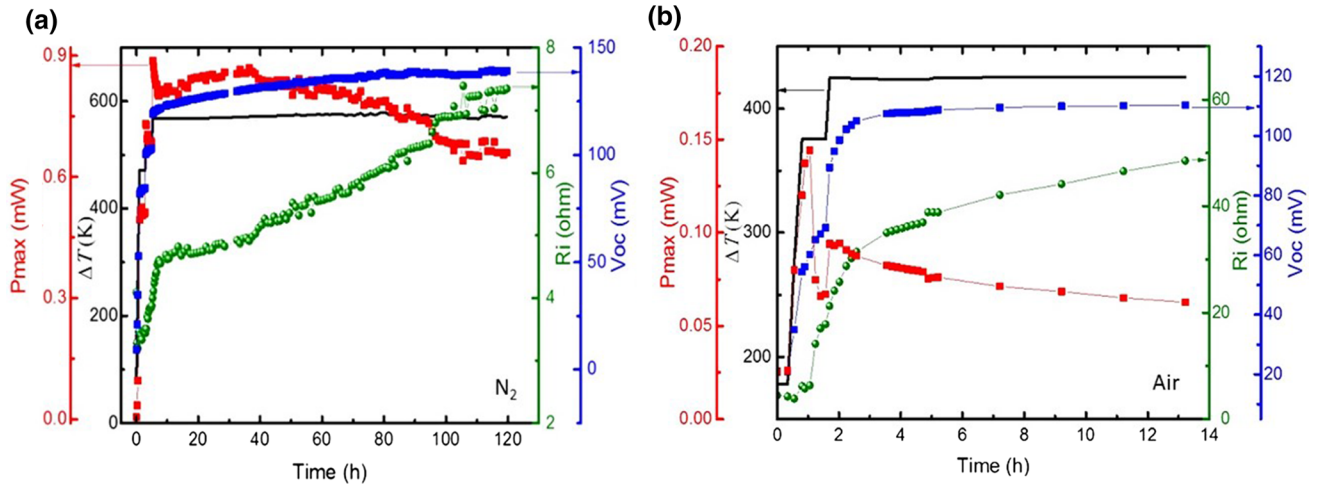

Fig. 1. Characterization of TE modules consisting of LSTO and CCO-SP ceramics in (a) N_2 and (b) air. The cold side of the modules was fixed slightly above ambient temperature.

Table I. TE properties of the modules after 1 and 10 h measured in N_2 (600°C hot side) and air (450°C hot side)

	P_{max} (mW)/(mW/cm^2)		V_{OC} (mV)		R_i (Ω)	
	1 h	10 h	1 h	10 h	1 h	10 h
N_2	0.82/4.3	0.85/4.45	122	125	4.6	4.8
Air	0.09/0.47	0.07/0.37	105	110	31	48

circuit voltage (V_{OC}), electrical resistance (R_{module} or R_i) and ΔT as a function of time are included. P_{max} is calculated according to Eq. 1.[21]

$$P_{max} = V_{OC}^2/4 \cdot R_i \quad (1)$$

In both atmospheres, P_{max} decreases, while R_i and V_{OC} increase 1–2 h after startup. In N_2 (Fig. 1a), P_{max} increases with increasing temperature reaching ~ 0.9 mW (4.7 mW/cm^2) at maximum ΔT, and maintaining 0.85 mW for about 40 h, followed by a decrease to 0.65 mW after 120 h. After 1 h of ramping and reaching 400°C (hot side) (ΔT = 370 K), P_{max} reaches a maximum of about 0.15 mW (0.8 mW/cm^2) in air, thereafter rapidly decreasing and reaching 0.07 mW after 1 h dwelling (Fig. 1b). At 450°C (hot side) (ΔT = 420 K) P_{max} slightly increased from 0.07 to 0.09 mW, but during 12 h dwelling dropped to 0.06 mW.

Comparing P_{max} and R_i in the two atmospheres (Table I), significant differences are observed, which are attributed to oxidation of the as-sintered LSTO ceramics during the testing. The reduced performance of the module in air between 1 h and 10 h (Table I), is rationalized by the oxidation of LSTO (relative density ~ 84%) followed by a reduction in the electrical conductivity, corresponding to enhanced R_i. Since V_{OC} increases with the temperature gradient, power output reaches a maximum value at maximum temperature gradient with hot-side temperature at 600°C.

At high temperatures, the electrical conductivity of $SrTiO_3$-based materials is governed by small polaron hopping, defined by the ratio between Ti^{4+} and Ti^{3+}.[22] The shift in the ratio between the valence states of Ti with increasing oxygen content is visualized by the chemical defect equilibrium described in Eq. 2.

$$V_O^{\cdot\cdot} + \frac{1}{2}O_2 + 2e' = O_O^{\times} \quad (2)$$

where O_o^x, $V_O^{\cdot\cdot}$ and e' respectively represent oxygen on an oxygen site, an oxygen vacancy, and electrons, the latter represents the Ti^{3+} state. Hence, oxidation of LSTO will shift the defect equilibrium in Eq. 2 to the right and reduce the fraction of Ti^{3+} corresponding to a reduced electrical conductivity. Hence, the electrical conductivity of LSTO will decrease with oxidation, which goes in favor of enhanced thermopower and V_{OC}. Substituting Sr with La (donor dopant) will enhance the electric conductivity;[23] however, at the temperatures and atmospheres given in our investigation, the relative change in conductivity is adequately explained by Eq. 2.[19] Thus, the combination of the specific *n*- and *p*-type TE materials chosen here is challenging even for low-temperature applications in air.

There are also issues with the stability of the metallic interconnect. Figure S1 (Supplementary data) shows a tiny increase in the observed operating voltage with time which is interpreted as the formation of cracks or exfoliation of the Ag-paste, leading to less electrical contact between the active components. Although only a minor change in voltage, these processes must also be considered when optimizing the design of the TE module.

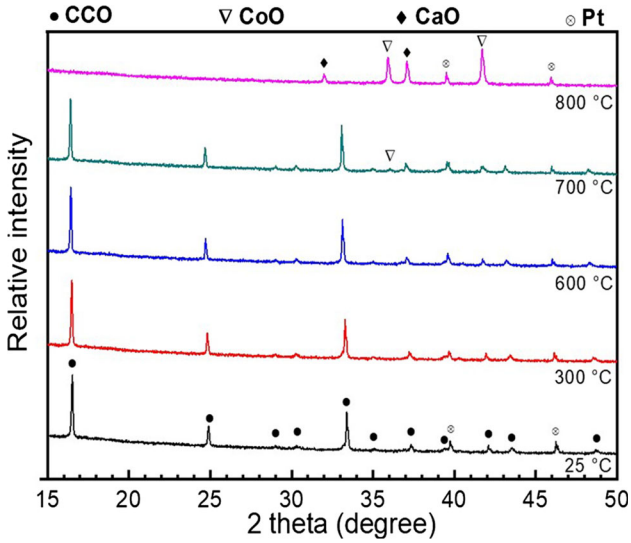

Fig. 2. HT-XRD patterns of CCO-SSR powder recorded in N_2 with 30 min dwell at each temperature. Diffraction lines of the Pt strip used for heating is observed at all temperatures.

Table II. Temperature ranges of stability of CCO in O_2, air and N_2. Data for O_2 and air are taken from Ref. 15

	In situ HT-XRD (powder)		
	O_2 (°C)	Air (°C)	N_2 (°C)
Upper limit phase purity	950–975	925	600–700
Decomposition	975	925–950	~ 700
Observed up to	1000	950	700

Material Stability in N_2 and Air

Figure 2 shows HT-XRD of CCO-SSR powder in N_2 between room temperature and 800°C, while XRD of LSTO is presented in the Supplementary data (Fig. S2). SSR powder is used for HT-XRD analysis in order to obtain more intense reflections compared to significantly less crystalline SP powder that was used for the module. We start with phase-pure CCO, and at 600°C phase-pure CCO is still present, while at 700°C decomposition is initiated as shown by the weak reflection corresponding to CoO. However, at 800°C, CCO is completely decomposed to CaO and CoO solid solutions, leaving the decomposition of the intermediate $Ca_3Co_2O_6$ phase[15] undefined between 700°C and 800°C. Since HT-XRD of CCO powder in N_2 was performed at the same conditions as reported in Ref.15, the obtained results are directly comparable, and the temperature stability ranges of CCO in three different atmospheres are summarized in Table II.

Here we see that a TE module exposed to a maximum hot-side temperature of e.g. 700°C in N_2 may be followed by decomposition of CCO corresponding to severe deterioration of the performance of the TE module.

Thermogravimetric analysis in N_2 and air of ground CCO-SP and LSTO ceramics is presented in Fig. 3. A negligible mass loss of CCO-SP in region I (below 200°C) is related to adsorbed moisture (Fig. 3a). A notable mass loss is observed in region II above 550°C, as well as a significant difference in mass loss between the two atmospheres in region III above 700°C (Fig. 3a).

A change in mass of about 2% in region II is related to reduction of Co_3O_4 secondary phase to $Co_{1-x}O$,[24,25] and further (in region III) into CoO, while negligible mass loss below 700°C in air of the stoichiometric CCO-SSR (with no Co_3O_4 secondary phase) is shown in the inset of Fig. 3a for comparison. This points to an imperfection in the previously reported miscibility region (Ca:Co ratio lying between 0.74 and 0.76).[18] Besides a notable Co excess and formation of Co_3O_4 in CCO-SP, a very small Co excess within the narrow miscibility region leads to formation of Ca defects and additional p-type charge carriers in phase pure CCO that increase zT.[26] Different mass loss in two atmospheres in region III (Fig. 3a) is attributed to significant differences in the oxidation states of Co in CCO; hence, a notable change in oxygen non-stoichiometry (δ) is more pronounced in an atmosphere with lower pO_2 (N_2). Two plateaus in region III are observed in air at about 900°C and 1000°C corresponding to CCO (≈ 930°C) and $Ca_3Co_2O_6$ (≈ 1050°C) decomposition temperatures,[15] while in N_2 a continuous mass loss is observed, probably due to the narrow temperature range between the two decomposition temperatures of CCO (≈ 700°C) and $Ca_3Co_2O_6$ (700–800°C). Furthermore, a mass change of about 7.6% in region III corresponds to full decomposition of CCO into CaO and CoO solid solutions, which is in good agreement with a previous report.[14] The δ of the as-sintered CCO-SP ceramic at the beginning of thermogravimetric analysis is calculated to be ~ 0.17. Since fully oxidized material is expected to have $\delta \sim 0.36$,[14] then $\delta \sim 0.17$ indicates a reduced oxygen content due to the reducing (vacuum) conditions during sintering in SPS.

Thermogravimetric analysis in N_2 and air of ground and bulk LSTO ceramic is presented in Fig. 3b. More pronounced mass change is observed in as-sintered bulk LSTO in air than in ground LSTO in N_2, as explained by Eq. 2 (equilibrium shifted to the right). Traces of O_2 were present during the analysis in N_2; therefore, a slight increase in mass is observed. The O_2 concentration in the N_2 atmosphere during the module test (Fig. 1a) is probably higher than that in the N_2 atmosphere used in TG analysis (Fig. 3b), due to less efficient removal of oxygen by flushing. It is expected that the TE module will produce high power output significantly longer than 40 h, given a

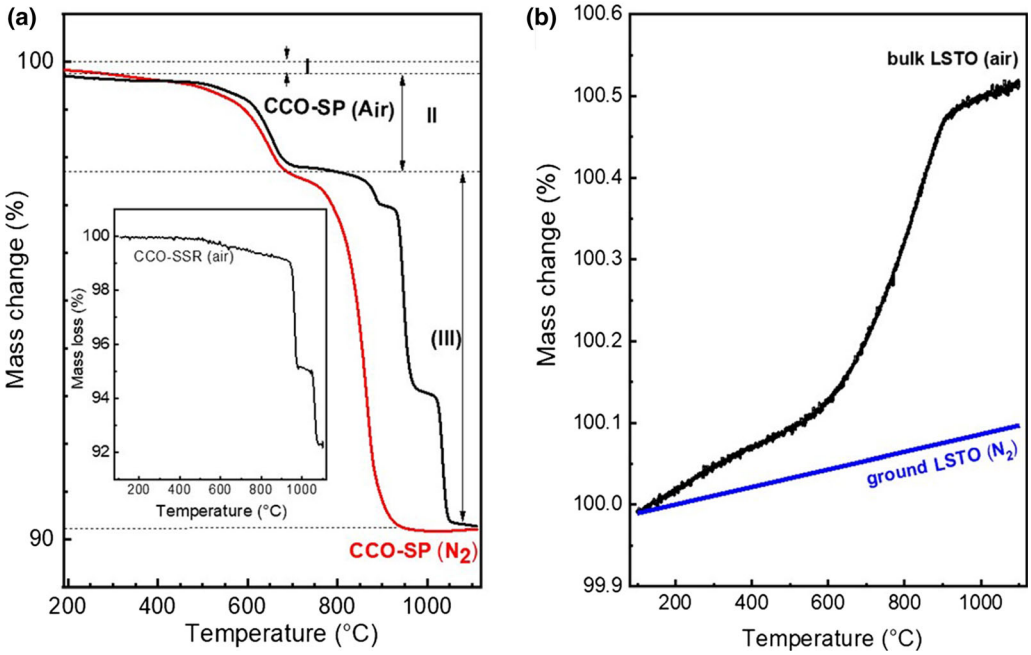

Fig. 3. Thermogravimetric analysis in N_2 and air: (a) of ground CCO-SP ceramics (inset represents a mass loss of pure CCO-SSR powder in air) and (b) of ground and bulk LSTO-SSR ceramics.

high-purity N_2 atmosphere during testing. Oxidation of the as-sintered bulk LSTO in air demonstrated a notable mass increase. The rate of oxidation was partly enhanced by the 8% open porosity in LSTO; however, a detailed assessment of the oxidation kinetics lends itself to a more elaborate analysis including the measurements of oxygen surface exchange and bulk diffusion. This is beyond the scope of the present investigation.

In general, besides the relatively low decomposition temperature of CCO, oxidation of LSTO is challenging, and enhanced performance of the module may be realized by applying an oxygen diffusion barrier (encapsulation) to the LSTO to suppress oxidation and maintain high electronic conductivity. Identifying an effective diffusion barrier compatible with LSTO will significantly boost the performance of the TE module and enable operation in ambient atmosphere at high temperatures.

CONCLUSIONS

TE modules consisting of a pair of *n*-type $(La_{0.12}Sr_{0.88})_{0.95}TiO_{3-\delta}$ and *p*-type $Ca_3Co_{4-x}O_{9+\delta}$ ceramic legs were tested in N_2 and air. The main challenge with the selected material system was the combination of materials having their optimum TE performance at different operating conditions. The TE modules demonstrated higher stability in N_2 (600°C) than in air (450°C). Maximum electrical power output of ~ 0.9 mW (4.7 mW/cm^2) at 600°C and $\Delta T \sim 570$ K in N_2 decreased after 40 h and stabilized at 0.65 mW after 120 h, while in air, output of ~ 0.15 mW (0.8 mW/cm^2) at 400°C and $\Delta T \sim 370$ K decreased after 1 h. Hence, a stable TE module operating in N_2 atmosphere was established although with a moderate power output. Operation of the module in ambient air needs to protect the LSTO from oxidation, for example, by applying a surface coating (sealant) impermeable to oxygen.

ACKNOWLEDGMENTS

Open Access funding provided by NTNU Norwegian University of Science and Technology incl St. Olavs Hospital - Trondheim University Hospital. We gratefully acknowledge financial support from the Research Council of Norway under the program Nano2021 to the project (number 228854) “Thermoelectric materials: Nanostructuring for improving the energy efficiency of thermoelectric generators and heat-pumps” (THELMA) conducted by NTNU, UiO, SINTEF, FFI, UiS and UiA. Dr. Magnus Rotan (NTNU) is acknowledged for technical support on HT-XRD. We also thank the Deutsche Forschungsgemeinschaft (DFG, German Research Foundation)—FE928/17-1 for the financial support.

OPEN ACCESS

ELECTRONIC SUPPLEMENTARY MATERIAL

The online version of this article (https://doi.org/10.1007/s11664-020-08127-5) contains supplementary material, which is available to authorized users.

REFERENCES

1. D. Milić, A. Prijić, Lj Vračar, and Z. Prijić, *Appl. Therm. Eng.* 121, 74 (2017).
2. D. Tainoff, A. Proudhom, C. Tur, T. Crozes, S. Dufresnes, S. Dumont, D. Bourgault, and O. Bourgeois, *Nano Energy* 57, 804–810 (2019).
3. K. Jaakkola and K. Tappura, *IEEE Sens. J.* 18, 7193 (2018).
4. M. Guan, K. Wang, D. Xu, and W.-H. Liao, *Energy Convers. Manag.* 138, 30 (2017).
5. G. Gromov, *Advanced Micro and Nanosystems* (New York: Wiley, 2017).
6. M. Ohtaki, K. Araki, and K. Yamamoto, *J. Electron. Mater.* 38, 1234 (2009).
7. L. Bocher, M.H. Aguirre, D. Logvinovich, A. Shkabko, R. Robert, M. Trottmann, and A. Weidenkaff, *Inorg. Chem.* 47, 8077 (2008).
8. Z. Lu, H. Zhang, W. Lei, D.C. Sinclair, and I.M. Reaney, *Chem. Mater.* 28, 925 (2016).
9. M. Bittner, N. Kanas, R. Hinterding, F. Steinbach, J. Räthel, M. Schrade, K. Wiik, M.-A. Einarsrud, and A. Feldhoff, *J. Power Sources* 410, 143 (2019).
10. A.C. Marques, Ph.D. thesis, Faculdade de Ciências da Universidade de Lisboa, Portugal (2009).
11. R. Boston, W.L. Schmidt, G.D. Lewin, A.C. Iyasara, Z. Lu, H. Zhang, D.C. Sinclair, and I.M. Reaney, *Chem. Mater.* 29, 265 (2017).
12. S. Funahashi, T. Nakamura, K. Kageyama, and H. Ieki, *J. Appl. Phys.* 109, 124509 (2011).
13. D. Sedmidubsky, V. Jakes, O. Jankovsky, J. Leitner, Z. Sofer, and J. Hejtmanek, *J. Solid State Chem.* 194, 199 (2012).
14. J. Shimoyama, S. Horii, K. Otzschi, M. Sano, and K. Kishio, *Jpn. J. Appl. Phys.* 42, 194 (2003).
15. N. Kanas, S.P. Singh, M. Rotan, M. Saleemi, M. Bittner, A. Feldhoff, T. Norby, K. Wiik, T. Grande, and M.-A. Einarsrud, *J. Eur. Ceram. Soc.* 38, 1592 (2018).
16. X.-D. Zhou, L.R. Pederson, E. Thomsen, Z. Nie, and G. Coffey, *Electrochem. Solid State* 12, 2 (2009).
17. F. Delorme, P. Diaz-Chao, E. Guilmeau, and F. Giovannelli, *Ceram. Int.* 41, 10038 (2015).
18. E.M.M. Ibrahim, L.H. Abdel-Rahman, A.M. Abu-Dief, A. Elshafaie, S.K. Hamdan, and A.M. Ahmed, *Mater. Res. Bull.* 99, 103 (2018).
19. S.P. Singh, N. Kanas, T.D. Desissa, M.-A. Einarsrud, M. Johnsson, T. Norby, and K. Wiik, *J. Eur. Ceram. Soc.* 40, 401 (2020).
20. G. Skomedal, T. Vehus, N. Kanas, S.P. Singh, M.-A. Einarsrud, K. Wiik, and P.H. Middleton, *Mater. Today Proc.* 8, 696 (2019).
21. E. Guilmeau, D. Berardan, C. Simon, A. Maignan, B. Raveau, D. Ovono Ovono, and F. Delorme, *J. Appl. Phys.* 106, 053715 (2009).
22. R. Moos, W. Menesklou, and K.H. Härdtl, *Appl. Phys. A* 61, 389 (1995).
23. R. Moos and K.H. Härdtl, *J. Am. Ceram. Soc.* 80, 2549 (1997).
24. V. Bartunek, Š. Huber, D. Sedmibudsky, Z. Sofer, P. Šimek, and O. Jankovky, *Ceram. Int.* 40, 12591 (2014).
25. M. Chen, B. Hallstedt, and L.J. Gauckler, *J. Phase Equilib.* 4, 212 (2003).
26. G. Buttner, S. Populoh, W. Xie, M. Trottman, J. Hertrampf, M. Dobeli, L. Karvonen, S. Yoon, P. Thiel, R. Niewa, and A. Weidenkaff, *J. Appl. Phys.* 121, 215101 (2017).